ELSEVIER

Journal of Molecular Catalysis A: Chemical 149 (1999) 179–195

JOURNAL OF MOLECULAR CATALYSIS A: CHEMICAL

www.elsevier.com/locate/molcata

Spin uncoupling in molecular hydrogen activation by platinum clusters

Boris Minaev *, Hans Ågren

Department of Physics and Measurement Technology, Linköping University, S-58 183 Linköping, Sweden

Received 14 December 1998; accepted 23 February 1999

Abstract

Complete active space multiconfiguration self-consistent field (CAS-MCSCF) and multireference configuration interaction (MRCI) calculations for H_2 reactions with platinum atom and small clusters (Pt_2, Pt_3) have been performed with account of spin-orbit coupling (SOC). Relativistic effective core potential basis sets are used. It is shown that the $^3D_2$ state of the Pt atom, which is only 2.2 kcal/mol higher in energy than the ground state component, $^3D_3$, is reactive in hydrogen insertion reactions. The activation barrier (about 2 kcal/mol) is formed by a very efficient singlet–triplet (^1S–$^3D_2$) avoided crossing determined by SOC in the $5d$ shell of the metal, and a very stable singlet $^1A_1$ ground state product PtH_2 is produced by Pt($^3D_2$) atom insertion into the hydrogen. Despite of the fact that asymptotic states in the entrance channel differ by 2 in angular momentum quantum number, a small mixing between the ^1S and ^1D states obtained at the MRCI level at the beginning of the reaction leads to a drastic change in the j–j coupling scheme and finally produces the S–T intersystem crossing. Other states are nonreactive, since they have a barrier higher than 15 kcal/mol. A simple concerted insertion of platinum dimer into H_2 molecule is studied in order to simulate spin uncoupling produced by CI between the ground singlet state of the reactants and the double–triplet state $^1[Pt_2(^3\Sigma_g^-) + H_2(\Sigma_u^+)]$. This type of spin uncoupling is typical for all studied reactions even when they do not follow the concerted mode. The triplet–singlet intersystem crossing occurs at the tight chemical interaction stage for cluster reactions in contrast to activation by a bare atom.

Keywords: Hydrogen; Platinum; Spin uncoupling

1. Introduction

Activations of chemical bonds in stable diamagnetic molecules by transition metal (TM) atoms, clusters and complexes have been extensively studied both by experimentalists and theoreticians during the last decade. The fast development of powerful experimental techniques like molecular and ion beams in combination with laser flash-photolysis and mass spectroscopy has provided a huge amount of important information about TM atoms, clusters and ion reactivity with stable molecules. Reactivity of TM species in different spin states is a most important issue with respect to the basic understanding of catalytic processes, both homogeneous and hetero-

* Corresponding author

1381-1169/99/$ - see front matter
PII: S1381-1169(99)00173-9

geneous. The simplest question in this respect is: Why can the TM atom, cluster or complex easily bind a stable molecule and then easily release it in some active form for subsequent chemical transformations in which the TM species does not participate in the sense that it does not enter the final product? Do electron spins play any particular role in these processes? Many useful concepts have been proposed accounting for the peculiarity of *d* orbitals, like $d \rightarrow$ LUMO donation and $s \leftarrow$ HOMO back donation [1], *sd*-hybridization [2,3], the promotion energy to the bonding s^1 state [4,5], etc. However, not so much attention has been devoted to spin effects in catalysis so far [6–10].

Chemical reactions are strongly spin-dependent because of the importance of the exchange energy. The correlation effects in *d* shells of TM species have been well studied and documented [2–5,11], stressing in particular the dependence of the reactivity on multiplicity [10]; but still there are many other aspects of the TM spin chemistry which have not received proper attention.

It is well known that such stable diamagnetic molecules like H_2 and alkanes are rather easily activated by partially coordinated unsaturated metal centers in many metallo-organic complexes [2,12] and clusters [13,14]. Great efforts towards first principles investigations of the mechanisms for these processes were undertaken by Siegbahn et al. [3], Blomberg et al. [4,5], Wittborn et al. [11], Low and Goddard [2,15], Balasubramanian [8,17,18], Balasubramanian et al. [16] and by Koga and Morokuma [19], Musaev and Morokuma [20] and Cui et al. [21,22], who determined the variation of metal–molecule binding energies for different metals, molecules and reaction coordinates.

Hydrogenation, i.e., the addition of molecular hydrogen to unsaturated hydrocarbons such as olefins, is a reaction of great importance. Homogeneous hydrogenation catalysts are known for many TMs [12], of which platinum is one of the most important [17]. One of the roles of the catalyst is to activate the H_2 molecule, i.e., to break the H–H bond via the oxidative addition of the hydrogen to the metal complex. The oxidative addition reactions of the hydrogen molecule are now studied for a number of bare TM atoms and TM clusters in molecular beams using detection techniques involving single-photon ionization and time-of-flight mass spectrometry [13]. The oxidative addition of hydrogen to the platinum atom is one of the simplest prototype reactions involving unsupported Pt clusters [13,14].

The electronic states and potential energy surfaces (PES) of the PtH_2 system have been studied by many authors [2,8,7,21,23,24]. Poulain et al. [23] carried out pseudopotential SCF CI calculations from which they concluded that a triplet ground state of the Pt atom cannot capture H_2, since the two triplet states studied both have repulsive interaction. However, the singlet closed shell state $^1A_1$ inserts into the H–H bond without activation energy [23]. Similar results were obtained by GVB-CI calculations [2]. Since spin–orbit coupling (SOC) were not taken into account in these works [2,23], it was not possible to make an assessment of the reactivity to real states of the Pt atom.

Balasubramanian [8,16,25] has calculated the PtH_2 system using the complete active space MCSCF (CAS-MCSCF) method followed by multireference singles and doubles configuration interaction (MRSDCI) and relativistic CI. In these sophisticated studies, only a bending PES was analyzed. The dissociation limit $Pt + H_2$ could be obtained only at small bending angle $\theta \simeq 10°$. Singlet state PES calculations without SOC account demonstrated a clear potential barrier at the bending angle $\theta \simeq 20°$ (Fig. 2 in Ref. [8]) with $E_a \simeq 5$ kcal/mol. SOC diminishes this barrier only slightly as it is seen from Fig. 2 in Ref. [8]. At the same time, the spontaneous insertion of the $Pt(^1S_0)$ atom into H_2 to form $PtH_2(^1A_1)$ was predicted by Poulain et al. [23] in their CI treatment, by Low and Goddard [2] using the GVB method and by Swang et al. [24] using the MCSCF approach.

So the barrier on the singlet state PES shown in Ref. [8] seems to be an artifact of the reaction path simulation of the bending mode. The $Pt + H_2 = PtH_2$ reaction has also recently been studied by Cui et al. [21] using density functional theory (DFT). There is no comment on the activation barrier; the binding energy of H_2 to the $Pt(^1S)$ atom is 47.8 kcal/mol (the best estimation with account of the zero point correction) which is in qualitative agreement with all previous calculations [2,8,23,24].

Since the ground state of the platinum atom is a triplet d^9s^1 (^3D) state which has a high barrier for hydrogen insertion [2,8,23,24], a curve crossing to the singlet state is required, and the minimum crossing point can be viewed as the transition state for the activation process starting from the ground ^3D state atom reaction [21]. An avoided crossing between the singlet and triplet states can occur with account of the SOC which is quite strong in the Pt atom [26]. Balasubramanian [8] accounted for SOC in this reaction using a relativistic configuration interaction scheme for PtH^+, the d orbital population of which is close to that of PtH_2 and thus enables calculations of SOC splittings for electronic states of PtH_2. Balasubramanian [8] estimated SOC energy corrections to the singlet bent ground state $^1A_1$ and to the triplet linear H–Pt–H product. He also presented the lowest singlet and triplet state potentials with account of SOC as a function of the bending angle (Fig. 2 in Ref. [8]). The lowest triplet state in the Pt atom is the $^3D_3$ multiplet; in Fig. 2 of Ref. [8], there is no avoided crossing between the lowest singlet and triplet potential curves. Both curves cross each other at the angle $\theta \sim 25°$. It could be concluded that the triplet ground state of the Pt atom is nonreactive with respect to the hydrogen molecules and probably to other diamagnetic molecules like methane, since the nature of the H–H and C–H chemical bonds is quite similar.

Nakatsuji et al. [7] studied reactions of a hydrogen molecule with the Pt atom and with the small clusters Pt_2, Pt_3 by symmetry adapted cluster (SAC) and SAC-CI methods. The effect of SOC was examined for the Pt–H_2 system by account of one-electron SOC integrals on the Pt atom only with wave functions obtained at the Hartree–Fock (HF) and single excitation CI level [7]. Unfortunately, Nakatsuji et al. [7] did not make an assignment of the PES at the dissociation limit to the states of the Pt atom. An analysis of the potential energy curves calculated with account of SOC (Fig. 7 in Ref. [7]) and of the degeneracy of states at the dissociation limit makes this assignment rather difficult though. If the lowest state in Fig. 7 of Ref. [7] is the $^3D_3$ term of the Pt atom, it should be sevenfold degenerate, but it is only fivefold in this figure. If the next state is $^3D_2$ (its fivefold degeneracy corresponds exactly to the expectation), then the splitting between the two states ($E(^3D_2) - E(^3D_3)$) is too high (about 6300 cm^{-1} in Fig. 7 of Ref. [7], compared to 776 cm^{-1} from experimental data [26]). Other states in Fig. 7 of Ref. [7] are also difficult for interpretation both from the energetic and degeneracy arguments. No definite conclusions about the mechanisms of spin uncoupling in hydrogen activation by platinum atom was reached, while the role of SOC and triplet states were downplayed. So from both papers [7,8], the message seems to be that SOC is not of much importance for the $Pt + H_2$ reaction and that only the singlet $^1A_1$ state is reactive. The same result has been obtained (without account of SOC) in Refs. [2,23,24]. Poulain et al. [23] proposed that the ground state $Pt(^3D)$ atom should be photoexcited in order to react. They noted that the transition to the desired singlet state is forbidden and that the UV–visible spectra show no trace of modification of the reaction in the matrix isolation experiment [23].

In this paper, we study the problem of the singlet–triplet crossing in the $Pt + H_2$ reaction in detail. The issue has a great importance for many reactions on platinum surfaces and on platinum clusters of different size. The Pt_n clusters up to $n = 4$ have triplet ground states, the reactivity of which differs from that of the

singlet excited states [27–29] so the problem of the spin flip is crucial for such catalytic activity [9,30]. Accounting for the results for the Pt atom, we shall briefly discuss the hydrogen molecule activation by Pt_2 and Pt_3 clusters. Hydrogenation reactions are of primary importance in this respect, but the C–H bond activation could also be relevant to the problem. Our preliminary results for methane activation by a platinum dimer support the crucial importance of the SOC effect in this process. The whole problem sorts under the general spin-catalysis concept discussed in Refs. [9,30]. The simplest prototype of catalytic reactions, $Pt + H_2$, demonstrates all these features.

2. Method of calculation

The relativistic effective core potential basis set of Stevens et al. [31] has been used in this work. The four inner (valence) shell orbitals ($5s$,$5p$) of the Pt atom have been frozen in the CAS-MCSCF and in multireference configuration interaction (MRCI) calculations. Five doubly occupied $5d$ orbitals and one empty $6s$ AO were included in the CAS. The next three $6p$, one $7s$ and five $6d$ AOs were included in the MRSDCI calculations followed by relativistic MRCI + SOC calculations. This constitutes 9156 configuration state functions (CSFs) for singlet states and 13 650 CSFs for triplet states of the platinum atom. This type of MRCI was found to be relevant for the description of the 21 lowest singlet and triplet states of the platinum atom with account of the effective nuclear charge $Z_{\text{eff}}(\text{Pt}) = 1312$ for the one-electron SOC operator.

For the PtH_2 system, one additional $1\sigma_g$ MO of the hydrogen moiety was included in the CAS. The same number of empty platinum orbitals (which now are mixtures of platinum and hydrogen AOs) and the σ_u^* MO of the hydrogen moiety were used as the next 10 orbitals in the SOCI procedure of the GAMESS program [32]. The total number of CSFs is 21 378 for singlet and 32 886 for triplet states. All calculations have been performed with GAMESS code [33].

As a first step, we have performed geometry optimization at the restricted HF (RHF) level for the singlet states and at the restricted open-shell HF (ROHF) level [34] for the triplet states. The geometry optimizations were thereafter performed at the MCSCF level; the CAS then included the σ_g MO of hydrogen and nine orbitals of the $5d6s6p7s$ shells of the Pt atom. So the CAS represents 11 orbitals for 12 electrons and constitutes a 15 492 configuration wave function (CSF) for the singlet state of the $^1A_1$ symmetry. Such optimization was performed only for the ground state product. All other CAS-MCSCF geometry searches were performed with three vacant MOs and six doubly occupied orbitals; this CAS includes $\sigma_g 5d6s$ + two $6p$ orbitals which are mixed with hydrogen AOs. Besides the ground singlet state, some other excited roots were optimized for different intermediates including the $^3B_2$ states. The simulation of the reaction paths has been performed accounting for some intermediate points from the geometry optimization search which started from a very long distance $d_{\text{Pt–H}} = 5$ Å at the C_{2v} symmetry. The choice of axes and distance notation are given in Fig. 1. Further simulation of the reaction paths has been performed by a point grid at the MRCI level. The most important region of the S–T crossing occurs at the early stage of the reaction [8] where there is no large distortion of the H–H bond length.

A few geometries have been calculated for the Pt_2 reactions with hydrogen and methane in a small CAS; it includes $\pi_g \delta_g \delta_u \sigma_u$ and two σ_g MOs of the platinum dimer with large contributions from $5d$ AOs. One bonding and one antibonding orbitals of the activated molecules for prolongated H–H and C–H bonds were also included. So the CAS consists of 11 orbitals for 16 electrons. The doubly occupied MOs $\sigma_g \pi_u$ of the Pt_2 dimer with energies -0.407 and -0.386 a.u. were excluded from the CAS

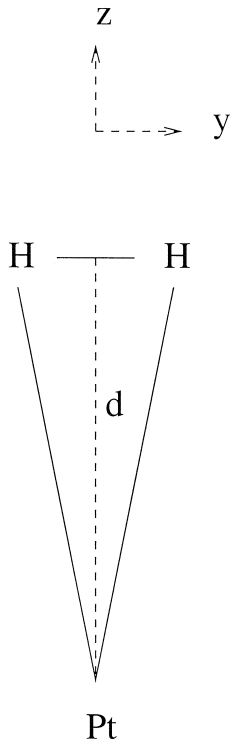

Fig. 1. The choice of axes for the $Pt + H_2$ reaction.

though they correspond to $5d$ AOs of platinum. Geometry optimization in this CAS of the singlet ground state gives *cis* and *trans* products of Pt_2H_2 very similar to that obtained by other authors [17,21]. MRCI calculations include the CAS of occupied $\pi_g \delta_g \delta_u \sigma_u$ and two σ_g MOs of the platinum dimer plus the σ_g MO of the H_2 molecule and one empty σ_g MO of Pt_2. Next 10 empty MOs are included in the second-order CI procedure. This gives 49 573 CSFs for the $^1A_1$ state in C_{2v} symmetry.

The SOC matrix elements have been calculated with the effective one-electron SOC operator in the framework of the GAMESS program [32]. The effective nuclear charge $Z_{\text{eff}}(\text{Pt}) = 1312$, intended to circumvent the need for the two-electron SOC integrals, have been adjusted to reproduce the results of the term splittings in the atomic spectra. For the carbon and hydrogen atoms, the effective SOC nuclear charges are compiled from Ref. [32]: $Z_{\text{eff}}(\text{C}) = 3.6$ and $Z_{\text{eff}}(\text{H}) = 1$. The final energies of states are obtained by diagonalization of the sum of the MRCI and SOC matrices in the GAMESS program [32]. All SOC calculations for the Pt atom and for the PtH_2 complex are done in the C_1 symmetry point group.

3. Results and discussion

3.1. The spectrum of the Pt atom

The orbital energies of the Pt atom calculated at the RHF ECP level are given in Table 1 together with MO energies of the PtH_2 system at two intermolecular distances. It is seen that the hydrogen molecular orbitals σ_g and σ_u at the beginning of the reaction ($n = 5$ and $n = 16$, respectively, in Table 1) get stabilized. There is an increase of electron density donation from the σ_g MO to the $6s$ AO of the Pt atom ($n = 11$) as the intermolecular distance decreases. Quite similar electron transfer has been obtained at the CAS-MCSCF level. The back electron transfer from the $5d_{yz}$ orbital ($n = 8$ in the complex, Table 1) to the unoccupied σ_u MO of the H_2 moiety is also well seen at both computational levels. This electron transfer in both directions occurs even in the case when the H–H bond length is kept frozen. Such trends have been noted in previous studies [2,7].

The first CI calculations of the Pt atom and the Pt–H_2 system were performed at the CAS CI level. Besides the four inner shells frozen orbitals of the Pt atom, five doubly occupied $4d$ orbitals, one $5s$ and three $5p$ AOs were included in the CAS. The results of this CAS CI calculations (CAS for Pt atom consists of 5292 CSF for the singlet states and of 7560 CSF for the triplet states) are rather poor for the platinum atom itself. These nonrelativistic calculations give a negative value for the $^1S \leftarrow {}^3D$ transition energy which contradicts all other nonrelativistic calculations [2,7,21,23] and leads to disagreement with experimental energy levels [26] when SOC is included in the CI matrix.

Table 1
Calculated HF orbital energy levels (a.u.)[a] of the Pt atom and of the PtH_2 system in the singlet ground state. Mulliken population of Pt atom in the occupied orbitals[b]

Pt atom			PtH_2 system					
∞					3.62 Å		2.63 Å	
n'	C_{2v}	$Pt^1S(d^{10}s^0)$[a]	n	C_{2v}	$PtH_2(^1A_1)$[a]	Pt[b]	$PtH_2(^1A_1)$[a]	Pt[b]
1	a_1	−4.2994	1	a_1	−4.2982	2.00	−4.3005	2.00
2	a_1	−2.4686	2	a_1	−2.4677	2.00	−2.4720	2.00
3	b_1	−2.4686	3	b_1	−2.4673	2.00	−2.4679	2.00
4	b_2	−2.4686	4	a_1	−2.4673	2.00	−2.4678	2.00
			5	a_1	−0.5968	0.01447	−0.6147	0.05878
5	b_2	−0.3197	6	a_1	−0.3188	1.99866	−0.3182	1.98254
6	a_1	−0.3197	7	b_1	−0.3186	2.00	−0.3211	2.00
7	b_1	−0.3197	8	b_2	−0.3185	1.99981	−0.3206	1.99438
8	a_1	−0.3197	9	a_2	−0.3183	2.00	−0.3175	2.00
9	b_2	−0.3197	10	a_1	−0.3183	2.00	−0.3175	1.99912
10	a_1	0.0018	11	a_1	0.0050	0.00	0.0133	0.00
11	a_1	0.0906	12	b_2	0.0897	0.00	0.0860	0.00
12	b_2	0.0906	13	b_1	0.0909	0.00	0.0899	0.00
13	b_1	0.0906	14	a_1	0.1037	0.00	0.1249	0.00
14	b_1	0.1544	15	a_1	0.1588	0.00	0.1512	0.00
			16	b_2	0.2538	0.00	0.2537	0.00
15	a_1	0.3342	17	b_1	0.3343	0.00	0.3273	0.00
16	b_1	0.3342	18	a_1	0.3351	0.00	0.3367	0.00
17	b_2	0.3342	19	a_2	0.3551	0.00	0.3367	0.00
18	a_1	0.3342	20	a_1	0.3505	0.00	0.3824	0.00
19	a_2	0.3342	21	b_2	0.3597	0.00	0.3934	0.00

Much better agreement with experiment are obtained at the MRSDCI level (Table 2). The relativistic results (MRCI + SOC) are given in the third column of Table 2. The ^3D triplet state gets much lower, so that the nonrelativistic excitation $^1S \leftarrow {}^3D$ energy becomes positive (0.03 eV), which finally leads to a good agreement with the experimental energy levels when SOC is taken into account.

It is interesting to note that the energy gap $^1S \leftarrow {}^3D$ seems to be well reproduced even at the HF level. Our HF calculations give 0.9 eV, while the experimental S–T splitting $E(^1S) - E(^3D_3)$ is equal 0.76 eV (the S–T splitting for the second triplet sub-level $E(^1S) - E(^3D_2) =$ 0.67 eV is very close [26]). All researchers consider the experimental energy gap 0.76 eV as a measure of electron promotion energy

Table 2
Calculated energy levels of the Pt atom in the absence of SOC (MRCI result) and with account of SOC (MRCI + SOC method)

Term	MRCI (a.u.)	MRCI + SOC[a]	D[b]	Exp. (cm^{-1})[c]
$^3D_3[4d^9(^2D_{2.5})5s]$	−118.823370	0.00	7	0.000
$^3D_2[4d^9(^2D_{2.5})5s]$	−118.823370	2066.54	5	775.9
$^1S(d^{10}s^0)$	−118.822295	4646.12	1	6140.0
$^3D_1[4d^9(^2D_{1.5})5s]$	−118.823370	11 025.06	3	10 132.0
$^1D_2[4d^9(^2D_{1.5})5s]$	−118.807364	12 471.36	5	13 496.3

[a] In cm^{-1}.
[b] Degeneracy.
[c] Ref. [26].

$d^{10}(^1S) \leftarrow d^9s^1(^3D)$ in nonrelativistic calculations [2,7,21,23]. For example, Poulain at el. [23] stressed that the S–T energy difference $d^{10}(^1S) \leftarrow d^9s^1(^3D)$ is of crucial importance for the accuracy of their nonrelativistic calculations. The same attention was paid to the S–T gap energy in the Pt atom in other nonrelativistic studies [2,7,21]. The connection between the S–T energy gap and the nonrelativistic promotion energy $d^{10}(^1S) \leftarrow d^9s^1(^3D)$ was considered to be of crucial importance for the reactivity of the Pt atom, especially with respect to the Pd atom reactivity, where the $E(^1S) - E(^3D)$ gap is negative [21,25]. We need to stress here that the experimental $E(^1S) - E(^3D_3)$ energy gap (= 0.76 eV) for the Pt atom has not much in common with the nonrelativistic promotion energy $d^{10}(^1S) \leftarrow d^9s^1(^3D)$, since the gap is determined mostly by SOC (in contrast to the palladium atom [35]).

The proximity of the two spin-sublevels $^3D_3$ and $^3D_2$ is confusing, both are well separated from the ^1S state (they are lower by 0.76 and 0.67 eV, respectively); at the same time, the third spin-sublevel $^3D_1$ is higher in energy by 0.5 eV than the singlet ^1S term. The last circumstance seems to simply be ignored previously [2,7,21,23]. All ^3D_J terms have the same configuration d^9s^1. Why should the measure of the nonrelativistic promotion energy $d^{10}(^1S) \leftarrow d^9s^1(^3D)$ be the $E(^1S) - E(^3D_3)$ energy gap, but not the $E(^1S) - E(^3D_1)$ one? In order to solve this problem, it is necessary to calculate the SOC correction carefully.

We did not consider F and P states in the MRCI + SOC matrix (configurations d^8s^2 are much higher in energy in nonrelativistic MRCI and do not influence the lowest states during the reaction), but the results for the other lower states are qualitatively correct. The worst energy is obtained for $^3D_2$ term, which is overestimated by 0.16 eV (maybe because the $^3P_2$ state was excluded from consideration). At least we have reproduced correctly the sequence of levels $^3D_3$, $^3D_2$, $^1S_0$, $^3D_1$ and $^1D_2$. The most essential aspect is that the lowest T–S splitting between the $^3D_3$ ground term and the $^1S_0$ state is qualitatively correct, which is important for the chemical reactivity of the Pt atom. The interval for the upper $^3D_1$ and $^1D_2$ states is also qualitatively reproduced (Tables 3 and 4).

The most important splittings between spin sub-levels are qualitatively good (all values are in cm^{-1}, experimental intervals are in parentheses):

$E(^1S) - E(^1D_2) = -7825\ (-7356)$,
$E(^3D_2) - E(^3D_1) = -8958.5\ (-9356)$,
$E(^1D_2) - E(^3D_3) = 12\,471\ (13\,496)$.

Perfect degeneracy for all multiplets is obtained in the C_1 point group calculations with the GAMESS program, which makes credit to the method applied. Large deviations from the simple Lande interval rule are well reproduced. We must stress that there is no SOC between the ground ^1S state (which is considered to be responsible for the reaction [2,7,8,23]) and any of the other lowest 15 terms of the Pt atom.

Table 3
Calculated energy levels of the PtH_2 system at the distance $d = 3.3$ Å in the absence of SOC (MRCI result) and with account of SOC (MRCI + SOC method)

C_{2v}	Pt term[a]	MRCI (a.u.)	MRCI + SOC[b]
$^3A_1$	$^3D_3[4d^9(^2D_{2.5})5s]$	−119.95038	−4006.26
$^3A_1$	$^3D_3[4d^9(^2D_{2.5})5s]$	−119.94999	−4003.76
$^3A_1$	$^3D_3[4d^9(^2D_{2.5})5s]$	−119.94996	−4002.52
$^3B_1$	$^3D_3[4d^9(^2D_{2.5})5s]$	−119.94967	−3984.18
$^3B_1$	$^3D_3[4d^9(^2D_{2.5})5s]$	−119.94967	−3957.76
$^3B_2$	$^3D_3[4d^9(^2D_{2.5})5s]$	−119.94953	−3939.88
$^3B_2$	$^3D_3[4d^9(^2D_{2.5})5s]$	−119.94953	−3933.52
$^3B_2$	$^3D_2[4d^9(^2D_{2.5})5s]$	−119.94953	−1949.76
$^3B_1$	$^3D_2[4d^9(^2D_{2.5})5s]$	−119.94967	−1948.08
$^3A_2$	$^3D_2[4d^9(^2D_{2.5})5s]$	−199.68538	−1883.55
$^3A_2$	$^3D_2[4d^9(^2D_{2.5})5s]$	−199.68538	−1874.62
$^3A_2$	$^3D_2[4d^9(^2D_{2.5})5s]$	−199.68538	−1871.83
$^1A_1$	$^1S(d^{10}s^0)$	−119.95276	77.35
$^3A_1$	$^3D_1[4d^9(^2D_{1.5})5s]$	−119.94953	7015.27
$^3A_1$	$^3D_1[4d^9(^2D_{1.5})5s]$	−119.94953	7020.11
$^3A_1$	$^3D_1[4d^9(^2D_{1.5})5s]$	−119.94953	7038.59
$^1A_1$	$^1D_2[4d^9(^2D_{1.5})5s]$	−119.93310	8493.32
$^1B_2$	$^1D_2[4d^9(^2D_{1.5})5s]$	−119.93309	8493.74
$^1A_2$	$^1D_2[4d^9(^2D_{1.5})5s]$	−119.93178	8555.15
$^1B_1$	$^1D_2[4d^9(^2D_{1.5})5s]$	−119.93176	8556.25
$^1A_1$	$^1D_2[4d^9(^2D_{1.5})5s]$	−119.93157	8569.55

[a] Qualitative comparison.
[b] SOC correction in respect to the lowest ^1S (MRCI) level in cm^{-1}.

Table 4
Calculated energy levels of the PtH_2 system at the distance $d = 2.8$ Å in the absence of SOC (MRCI result) and with account of SOC (MRCI + SOC method)

C_{2v}	Pt term[a]	MRCI (a.u.)	MRCI + SOC[b]
$^3A_1$	$^3D_3[4d^9(^2D_{2.5})5s]$	−119.94923	−3204.64
$^3A_2$	$^3D_3[4d^9(^2D_{2.5})5s]$	−119.94773	−3153.99
$^3A_1$	$^3D_3[4d^9(^2D_{2.5})5s]$	−119.94772	−3117.26
$^3B_1$	$^3D_3[4d^9(^2D_{2.5})5s]$	−119.94702	−3104.41
$^3B_2$	$^3D_3[4d^9(^2D_{2.5})5s]$	−119.947668	−3088.30
$^3A_2$	$^3D_3[4d^9(^2D_{2.5})5s]$	−119.94773	−2972.39
$^3B_2$	$^3D_3[4d^9(^2D_{2.5})5s]$	−119.94668	−2966.81
$^3B_1$	$^3D_2[4d^9(^2D_{2.5})5s]$	−119.94702	−1271.81
$^3B_1$	$^3D_2[4d^9(^2D_{2.5})5s]$	−119.94702	−1089.92
$^3A_2$	$^3D_2[4d^9(^2D_{2.5})5s]$	−119.94773	−1088.96
$^3A_2$	$^3D_2[4d^9(^2D_{2.5})5s]$	−119.94773	−932.68
$^3A_1$	$^3D_2[4d^9(^2D_{2.5})5s]$	−119.94772	−912.57
$^1A_1$	$^1S(d^{10}s^0)$	−119.953666	584.65
$^3A_1$	$^3D_1[4d^9(^2D_{1.5})5s]$	−119.94923	7867.50
$^3A_1$	$^3D_1[4d^9(^2D_{1.5})5s]$	−119.94923	7911.32
$^3A_1$	$^3D_1[4d^9(^2D_{1.5})5s]$	−119.94772	7947.55
$^1A_1$	$^1D_2[4d^9(^2D_{1.5})5s]$	−119.93211	9388.09
$^1B_2$	$^1D_2[4d^9(^2D_{1.5})5s]$	−119.93210	9389.28
$^1A_2$	$^1D_2[4d^9(^2D_{1.5})5s]$	−119.93200	9528.78
$^1B_1$	$^1D_2[4d^9(^2D_{1.5})5s]$	−119.92985	9550.19
$^1A_1$	$^1D_2[4d^9(^2D_{1.5})5s]$	−119.9297	9573.47

[a] Qualitative comparison.
[b] SOC correction in respect to the lowest ^1S (MRCI) level in cm^{-1}.

3.2. Pt atom reaction with molecular hydrogen

3.2.1. General features of the $Pt + H_2$ reaction

Optimization of the reaction coordinates for different states have been performed by MRCI calculations on a grid of points. The reaction coordinates are different for the singlet and triplet states (and also between ^1S and ^1D states). We have chosen some intermediate reaction path which is close to the lowest singlet ^1S state behavior (deviation in the H–H bond length is not large). Since SOC calculations for a large variety of states (21 states are included in MRCI + SOC diagonalization) are very time consuming, we have chosen smaller number of grid-points in the relativistic optimization of the reaction paths. The latter optimized reaction coordinates are obtained rather different from the nonrelativistic ones. (By nonrelativistic calculations, we mean here MRCI calculations without account of SOC. This definition is not precise, since some relativistic effects are accounted for in optimizations using the ECP basis sets.) For the few lowest states, all reaction coordinates correspond to C_{2v} symmetry. Results of the MRCI nonrelativistic calculations at the beginning of the reactions are given in Fig. 2 for the reaction path which is intermediate between the ground singlet and the five triplet states. At this stage of the process, all reaction coordinates are quite similar and differ only by a small variation of the H–H bond length in the region 0.75–0.79 Å. Calculations with account of SOC are presented in Fig. 3. We have found that optimization of the reaction path at the HF level is not completely adequate even for the lowest singlet and triplet states.

The HF geometry optimization of the singlet ground state product PtH_2 gives two minima. One is in the entrance channel with a very short H–H distance ($r_{H-H} = 0.8715$ Å) and a long Pt–H bond length ($r_{Pt-H} = 1.6914$ Å, the angle is 29.86°). The heat of formation of the adduct is 10.7 kcal/mol. This weak complex was not obtained in the MRCI calculation. The second one corresponds to a real insertion product with a broken H–H bond: $r_{H-H} = 2.05$ Å. At the

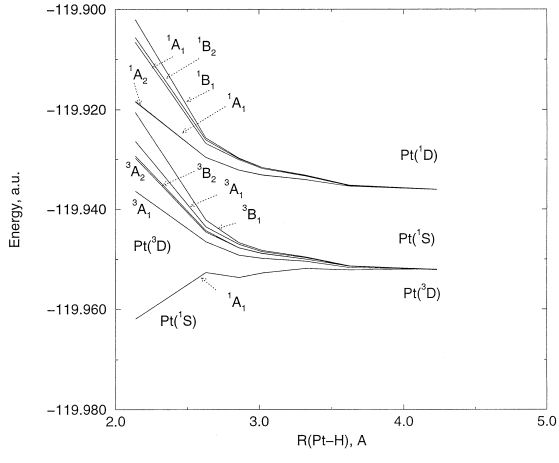

Fig. 2. Potential energy curves for the entrance channel of the reaction $Pt + H_2$ calculated by the MRCI method in the absence of SOC. At the starting point, the ^3D term is higher than the ^1S term by 242 cm^{-1}.

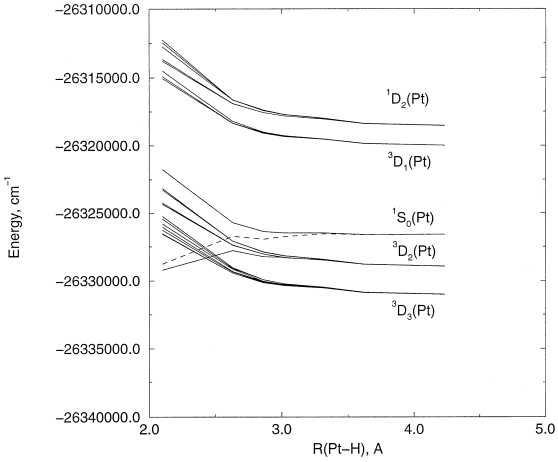

Fig. 3. Potential energy curves for the entrance channel of the $Pt+H_2$ reaction calculated by the MRCI method with account of SOC.

same time, the Pt–H bond length is very short $r_{Pt-H} = 1.534$ Å. The angle is 83.82°. This geometry is in a good agreement with Balasubramanian's results (2.056 and 1.52 Å and 85.1°, respectively) [8]. The heat of formation of the insertion product calculated at the HF and MRCI levels is 25.3 and 39 kcal/mol, respectively. The latter value is in good agreement with the SAC-CI result, obtained by Nakatsuji et al. [7] (40 kcal/mol).

Comparison of the two minima obtained at the HF level shows that the bonded valence [33] of the Pt atom is 0.856 for the weak complex and 1.918 for the insertion product (the hydrogen atom valence is 1.007 in both cases). There is no large difference in total atomic populations. The Pt atom has a small negative charge in both species (-0.12 in the first complex and -0.19 in the product). At the same time, the Mulliken's population of $5d_{zz}$ and $5d_{yz}$ orbitals is changed dramatically. The total population of the *s* AO is increased only slightly from 2.27 in the weak complex to 2.47 in the product. It means that the weak complex is a van der Waals adduct which does not include change of *s–d* hybridization and is obtained as an artifact of geometry optimization at the HF level. Account of CI leads to the mixing between d^{10} and d^9s^1 configurations which is responsible for the *s–d* hybridization which removes the local minimum.

The singlet–triplet vertical excitation in the insertion product is 2.8 eV for the A_1 symmetry. All triplet states of $^3A_1$ symmetry are unstable. They have a large barrier for insertion (at least more than 77 kcal/mol); if the lowest $^3A_1$ state overcomes the barrier, it descends to the linear molecule H–Pt–H. In this respect, our results completely reproduce CAS-MCSCF bending PES for the lowest $^1A_1$ and $^3A_1$ states obtained by Balasubramanian [8] with and without SOC inclusion; but the $^3B_2$ state, having a fast rising energy at the beginning of the reaction (Fig. 3), overcomes the barrier (36 kcal/mol) and produces a photostable excited product with the geometrical parameters $r_{Pt-H} = 1.646$ Å, $r_{H-H} = 2.964$ Å, $\gamma = 128.4°$ (CAS-MCSCF result). This $^3B_2$ pattern is the lowest excited state of the insertion product; the adiabatic excitation energy is 0.75 eV at the HF level and 1.56 eV at the MRCI level. The vertical excitation $^3B_2 \leftarrow {}^1A_1$ is equal 1.51 eV and 2.61 eV at both nonrelativistic levels, respectively. Inclusion of SOC to the MRCI calculation lowers the ground state energy by 328.1 cm^{-1} and yields a vertical excitation to the $^3B_2$ state equal to 2.31 eV. The zero field splitting of the lowest triplet state is about 90 cm^{-1}. The total energy of the three spin-sublevels are 18 337, 18 358.5 and 19 028.1 cm^{-1} with respect to the nonrelativistic ground state.

This photostable excited product ($^3B_2$) is separated from the linear one ($r_{Pt-H} = 1.689$ Å) by a barrier of 11 kcal/mol. The ground state of the linear product is $^1A_1(^1\Sigma_g^+)$ in the nonrelativistic HF and MRCI calculation ($r_{Pt-H} = 1.679$ Å). The triplet state $^3A_1(^3\Delta_g)$ is lowered in energy and becomes the ground state of the linear product when the SOC correction is included. This is also in agreement with the effect of SOC predicted in Ref. [8]. Account of SOC at the MRCI level does not change the conclusion about the photostable nature of the lowest excited $^3B_2$ state of the PtH_2 molecule though the

barrier for transformation to the linear isomer then gets lower (6.5 kcal/mol).

3.2.2. SOC effect in the $Pt + H_2$ insertion reaction

Since the ground state of the platinum atom is a triplet d^9s^1 (^3D) state which has a high barrier for hydrogen insertion [2,8,24], a curve crossing to the singlet state is required. The minimum crossing point can be viewed as the transition state for the activation process starting from the ground ^3D state atom reaction [21]. An avoided crossing between the singlet and triplet states can occur with account of SOC which is quite strong in the Pt atom [26]. Balasubramanian [8] accounted for SOC in this reaction using a relativistic configuration interaction scheme on PtH^+, the d orbital population of which is close to that of PtH_2 and for calculations of SOC splittings for electronic states of PtH_2. Balasubramanian [8] estimated the SOC energy corrections to the singlet bent ground state $^1A_1$ and to the triplet linear H–Pt–H product. He also presented the lowest singlet and triplet state potentials with inclusion of SOC as a function of the bending angle (Fig. 2 in Ref. [8]). The lowest triplet state in the Pt atom is the $^3D_3$ multiplet; in Fig. 2 of Ref. [8], there is no avoided crossing between the lowest singlet and triplet potential curves. Both curves cross each other at the angle $\theta \sim 25°$. It could be concluded that the triplet ground state of the Pt atom is nonreactive with respect to the hydrogen molecules.

As was mentioned before, in Balasubramanian's study of the electronic states and PES of the PtH_2 system, only the bending PES was analyzed. The dissociation limit $Pt + H_2$ could be obtained only at a small bending angle $\theta \simeq 10°$. The singlet state PES calculated without SOC demonstrates a clear potential barrier at the bending angle $\theta \simeq 20°$ (Fig. 2 in Ref. [8]) with $E_a \simeq 5$ kcal/mole. SOC only slightly diminished this barrier as it is seen from Fig. 2 in Ref. [8]. At the same time, the spontaneous insertion of the $Pt(^1S_0)$ atom into H_2 to form $PtH_2(^1A_1)$ was predicted by other authors [2,21,24]. Nakatsuji et al. [7] also calculated the SOC effect in the $Pt + H_2$ reaction, and presented an interesting PES picture, however, without assignments of states in the Pt atom dissociation limit.

In contrast to some earlier statements, we stress that SOC is the main driving force of the catalysis by platinum, as predicted by the present calculations. The most important region for spin uncoupling comprises the Pt–H_2 distances (d) between 3.0 Å and 2.6 Å on the reaction path. At these distances, the H–H bond length is almost unchanged at the HF level, but it starts to increase at the MRCI level. For example, at $d = 2.6$ Å, the optimized H–H bond length is 0.78 Å at the MRCI level and only 0.01 Å longer at the HF level. All reaction coordinates are very similar at large Pt–H distances. The H–H bond length ($r_e = 0.735$ Å) is only slightly increased (up till 0.74 Å) when the Pt–H distance diminishes from 5 Å till 3.6–3 Å.

The SOC matrix element between the ground singlet $^1A_1$ state and the lowest triplet state $^3A_1$ in the entrance channel is equal to zero by symmetry. An indirect mixing of these states can occur in the second order of perturbation theory and, of course, in the method used in this work (diagonalization of MRCI + SOC matrix); but we have not found any appreciable mixing of these two states for the whole reaction process. At the same time, the second ($^3A_2$), the fourth ($^3B_1$) and the fifth ($^3B_2$) excited triplet states (the order obtained from nonrelativistic MRCI calculations) have increasing values of SOC matrix element with the ground singlet state. In the reactants, all these matrix elements were zero, since all the five ^3D states (2^3A_1, $^3B_1$, $^3B_2$ and $^3A_2$ states in the C_{2v} group) were degenerate (in nonrelativistic CI method). The SOC matrix element between the ground singlet $^1A_1$ state and the triplet state $^3A_2$ is not very large during the reaction. At the beginning of the reaction ($r_{Pt-H} = 3.6$ Å), it is equal to 30 cm^{-1}. The SOC with the fourth triplet state,

$^3B_2$, is the highest (167 cm^{-1}). This state is only 0.008 eV higher in energy than the lowest triplet state. The next almost degenerate $^3B_1$ state produces a 146 cm^{-1} SOC integral. At the intermediate geometry ($r_{Pt-H} = 2.86$ Å), the SOC integrals between the ground singlet and these triplet states are equal to 49, 602 and 568 cm^{-1}, respectively. These matrix elements are comparatively large with respect to many SOC integrals for different ^3D components in the free Pt atom (typical value of 1800 cm^{-1}, the maximum value is 5240 cm^{-1}). It means that important s–p–d mixing occurs during the reaction. The s–p–d hybridization finally leads to appreciable SOC integrals between the ground singlet and excited triplet states. For the intermediate triplet state of the PtH_2 complex, which occurs at the early stage of the reaction, the ground singlet state lowering by SOC is 5.49 cm^{-1} from the MRCI + SOC calculation. This value is not important for the singlet ground state reaction of the Pt atom with hydrogen, but it indicates that for the triplet ground state reaction, the SOC effects could be crucial.

When the interaction between the Pt atom and hydrogen starts to grow, the orbital degeneracy is lifted. The splitting of states with different orbital symmetry calculated by the MRCI nonrelativistic method is not large. Nonrelativistic S–T crossing between the lowest triplet $^3A_1$ and singlet $^1A_1$ states occurs at $r_{Pt-C} = 4.23$ Å using the MRCI method, but the states are quite far separated when SOC is taken into account (-4422.5 cm^{-1} and $+2.01$ cm^{-1}, respectively). SOC splitting between seven components of the former $^3D_3$ ground term is in the range of 11 cm^{-1} at this intermolecular distance, but the structure of the wave functions is completely changed by a new complex mixing of the former configurations. The lowest singlet state of the $^1S(d^{10})$-type is only slightly perturbed by SOC (about 1%) at this distance.

At first glance, it seems quite natural to suspect that there is no effective intersystem crossing from the starting ^3D nonreactive state and the descending ^1S reactive state, since there is no SOC between pure atomic states. This is absolutely correct for the lowest $^3D_3$ components, but not completely correct for the next $^3D_2$ components, which are very close in energy [26]. There is strong mixing between the $^3D_2$ and $^1D_2$ states (these states are formed and strongly split by SOC interaction and constitute a complete mixture of some ^3D and ^1D nonrelativistic CSFs in the free Pt atom when SOC is included).

When the Pt–H_2 distance diminishes to 3 Å, a small rehybridization of singlet states starts to grow and the ground singlet $^1A_1$ state acquires an admixture of one of the ^1D components (the state number four among the singlets; it has the same $^1A_1$ symmetry and is separated by 0.64 eV). This state is determined mostly by the $5d_{zz} \rightarrow 6s$ single electron excitation. The admixture coefficient is only 0.095 at the Pt–H_2 distance $d = 3$ Å, and attains its maximum value 0.12 at $d = 2.8$ Å. At shorter distances ($d = 2.1$ Å), it again becomes smaller than 0.05. Because of that small admixture induced (MRCI calculations), the MRCI + SOC wave function of the $^1A_1$ state is changed drastically: now it is a complete mixture of the closed shell CSF and the ^1D and ^3D CSF's components when SOC is included. The MRCI + SOC calculation (Fig. 3) demonstrates this as a result of an avoided crossing between the ground singlet state ^1S (dashed line as obtained in the absence of SOC) and the lowest component of the $^3D_2$ state. The mechanism of this avoided crossing is rather peculiar. The closed shell contribution to the lowest $^3D_2$ state grows very fast; the coefficient is 0.4, 0.57, 0.66 and 0.94 at $d = 3$, 2.8, 2.6 and 2.1 Å, respectively. At the point $d = 3.2$ Å, this admixture is negligible. The intermolecular distance $d = 2.8$ Å represents a crucial point on the reaction coordinate. Starting from this point, the closed shell contribution to the lowest $^3D_2$ component prevails (33%) above the ^3D and ^1D contributions (none of them exceeds 20%) and this state energy is split by 200 cm^{-1} lower than the other $^3D_2$ components. It is still higher in energy than the seven $^3D_3$ components. The

other state with large singlet closed shell contribution (61%) has 1856 cm^{-1} higher energy.

At some longer Pt–H distance (3.35 Å), the structure of multiplets is still similar to the atomic splitting pattern: the cluster of seven states similar to the $^3D_3$ terms (from -4094.8 till -4030.3 cm^{-1} with respect to the nonrelativistic singlet ground state origin) and the cluster of five states similar to the $^3D_2$ terms (from -2011 till -1966.1 cm^{-1}) are easily assigned from the MRCI + SOC wave functions. The singlet closed shell state is only slightly perturbed; its energy is 61.7 cm^{-1} with respect to the nonrelativistic singlet ground state. All other $^3D_1$ and $^1D_2$ states are quite much separated in energy like in a free atom (Table VI).

So the S–T mixing, which starts to grow when the Pt–H distance diminishes up to 3 Å, is a very peculiar feature of SOC and exchange interaction in the platinum atom perturbed by the growing chemical bond with hydrogen. There is no H–H bond cleavage at this stage. It occurs only at a very short distance $d \simeq 1.3$ Å.

3.2.3. Three different stages of spin uncoupling in the Pt + H_2 reaction

We can divide the reaction path into three important hypothetical stages. These are not real kinetic stages, since they are not connected with well-pronounced minima on the PES (a very shallow minimum at $R = 2.82$ Å, Fig. 3, probably has no importance). These stages are connected with different phases of spin uncoupling during the H–H bond activation process.

The first stage could be called 'preparation of the catalyst' [30]. A weak intermolecular interaction (polarization of the electronic shell of the catalyst and starting hybridization) in the case of heavy metal catalyst can induce a strong recoupling in 'j–j' or 'λ–s' scheme, which leads to effective triplet–singlet transitions.

A very small admixture of the $^1D(d^9s^1)$ character into the closed shell $^1S(d^{10})$ configuration destroys the cluster structure of the atomic multiplets and splits off one of the $^3D_2$ components from the other components, making this $^3D_2$ component highly reactive with respect to chemical bonding with the H_2 molecule. It acquires an increasing singlet character and finally correlates with the singlet ground state of the PtH_2 product. This type of spin uncoupling proceeds entirely in the catalyst. A very strong SOC in the Pt atom is a driving force for the T–S transition, which is triggered by a weak intermolecular interaction.

The second stage of the Pt + H_2 reaction is determined by the other type of spin uncoupling (it is connected in some way with the first stage); this is a $5d \rightarrow 6s$ promotion with simultaneous partial electron transfer from σ_g (H_2) to $6s$ (Pt) and back donation from $5d$ of Pt atom to the empty σ_u MO of the hydrogen moiety. This stage could not be completely described at the HF level. Even CAS-MCSCF calculations with a small active space without inclusion of the second empty MO (the orbital number 11 of b_2 symmetry in Table 1) predict a stable local minimum at $R_{Pt-H} \simeq 1.7$ Å, $R_{H-H} \simeq 0.86$ Å and H–Pt–H angle $\simeq 25°$ as the HF calculations also do. This local minimum disappears at a larger CAS level and for MRCI calculations. The second MRCI root of the same $^1A_1$ symmetry has a minimum near this region, so it looks like an avoided crossing between two singlet states originating from the ^1D and ^1S terms of the Pt atom. This avoided crossing is seen on the PES presented by Poulain et al. [23].

The third stage starts to become important just after the crossing discussed above and provides a deep descent to the stable minimum of the insertion product. Spin uncoupling at this stage is determined by a very strong avoided crossing between the lowest singlet state of the tightly bound Pt–H_2 complex and an excited singlet state of two triplet particles

$$^{1,3,5}\left[{}^3D(\mathrm{Pt}) + {}^3\Sigma_u^+(\mathrm{H_2})\right]. \quad (1)$$

At a H–H internuclear distance equal to 4.8 Å and $d = 4$ Å, the energy of the singlet state is -119.81588 a.u. so the energy difference between this term and the lowest triplet

state dissociation limit $^3[^3D(\mathrm{Pt}) + {}^1\Sigma_g^+(\mathrm{H_2})]$ (-119.9520 a.u.) corresponds almost to the hydrogen dissociation energy (3.8 eV). The energy of the triplet counterpart of the state (Eq. (1)) is at the same geometry (119.81565 a.u.) so the S–T splitting is only 51 cm^{-1}. The singlet state of the triplet pair has the following wave function

$$^1\Psi_{A_1} = -0.206\psi_1 + 0.198\psi_2 - 0.442\psi_3 + 0.766\psi_4, \quad (2)$$

where

$$\psi_1 = |2200|, \ \psi_2 = |2020|, \ \psi_{3,4} = |1111|. \quad (3)$$

The order of orbitals in these determinants is $|\sigma_g, 5d_{yz}, 6s, \sigma_u|$, where $\sigma_{g,u}$ MOs are similar to the bonding and antibonding orbitals of the hydrogen molecule (other MOs are omitted here for simplicity). The ψ_3 and ψ_4 CSFs have the following spin pattern:

$$\psi_3 = \frac{1}{\sqrt{12}}\left[(\beta\alpha\beta\alpha) + (\beta\alpha\alpha\beta) + (\alpha\beta\alpha\beta) + (\alpha\beta\beta\alpha) - 2(\beta\beta\alpha\alpha) - 2(\alpha\alpha\beta\beta)\right], \quad (4)$$

$$\psi_4 = \frac{1}{2}\left[(\beta\alpha\beta\alpha) - (\beta\alpha\alpha\beta) + (\alpha\underline{\mathrm{et}}a\alpha\beta) - (\alpha\beta\beta\alpha)\right]. \quad (5)$$

The combination $-0.5\psi_3 + 0.866\psi_4$ corresponds to a pure state $^1[^3D(\mathrm{Pt}) + {}^3\Sigma_u^+(\mathrm{H_2})]$. A small admixture of the singlet H + H radical pair state $^1[^1S(\mathrm{Pt}) + {}^1\Sigma_g^+(\mathrm{H_2})]$ is present in the wave function (Eq. (2)). The triplet state $^3[^3D(\mathrm{Pt}) + {}^3\Sigma_u^+(\mathrm{H_2})]$ has no such admixture and this is the reason for the small S–T state splitting (Eq. (1)) at this distance. The singlet, triplet and quintet counterparts have different behavior along the reaction path; the singlet state produces the avoided crossing with the lowest singlet PES and provides the H–H bond cleavage in the product. The avoided crossing is well recognized in the CAS-MCSCF geometry optimization of the second root of $^1A_1$ symmetry. This type of avoided crossing is very prominent in the $Pt_2 + H_2$ reaction so we shall consider briefly this reaction below.

3.3. Hydrogen activation by platinum clusters

The avoided crossing between two types of $Pt_2 + H_2$ PES has been obtained by Balasubramanian [17]. One surface starts from the dissociation limit $Pt_2 + H_2$ at $d = 8$ Å; d here is a distance between the centers of the two molecules (Fig. 4) with the parallel mode of collision studied by Balasubramanian [17]. The second PES (the upper curve in Fig. 4) arises from the dissociation limit $Pt_2 + H + H$. This PES has been assigned to the $Pt_2(^1\Sigma_g^+) + H + H$ state [17]; however, we do not support this assignment here. There is another shortcoming of the study [17]; Cui at el. [21] showed recently that the parallel mode does not correspond to the optimum reaction path between the platinum dimer and the hydrogen molecule. The H_2 activation takes place preferentially at a single Pt atom first via a structure that is far from planar; then one of the hydrogen atoms migrates to the other metal center overcoming a negligible barrier [21]. At the moment, we shall not pay

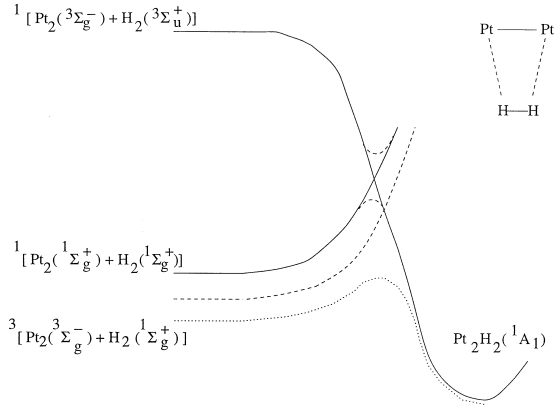

Fig. 4. Correlation diagram for the $Pt_2 + H_2$ reaction. The dashed and dotted lines correspond to the triplet surface, the solid lines — to the singlet ones. The dashed line corresponds to the absence of SOC. The dotted line corresponds to the account of SOC.

attention to the optimum reaction path for the hydrogen activation by the platinum dimer, but shall consider the parallel concerted approach (Fig. 4) as a simple simulation of a hypothetical route. The parallel mode of reaction, which needs to overcome an appreciable activation barrier, $\simeq 20$ kcal/mol [17], is very instructive for analysis of spin uncoupling in the system. The schematic correlation diagram for the parallel approach of the $Pt_2 + H_2$ molecules is shown in Fig. 4. We have calculated few points in this diagram and completed MRCI calculations including SOC as will be presented below. We stress that we have reproduced the main features of Balasubramanian's calculations [17], the only difference is connected with the upper curve assignment.

The Pt_2 cluster is predicted to have a triplet ground state from the nonrelativistic CAS-MCSCF calculations [7,21,36]. This is the $^3\Sigma_g^-$ state with the π_g^2 configuration (like for the O_2 molecule). A large number of states with low excitation energy (≤ 0.5 eV) have been obtained; the nearest one is the $^3\Pi_u$ state [21,36]. The lowest singlet state $^1\Sigma_g^+$ is only 0.35 eV higher in energy (MRCI calculation without SOC) in agreement with the nonrelativistic calculations (0.22 eV [36], 0.38 eV [21]). An account of SOC leads to a very strong repulsion between the $^3\Sigma_g^-$ and $^1\Sigma_g^+$ states (the energy difference between these states at $R_{Pt-Pt} = 2.44$ Å is 1.35 eV, which is similar to the $^3\Sigma_g^- - {}^1\Sigma_g^+$ splitting in the oxygen molecule determined by exchange interaction. The lowest triplet state surface obtained in the absence of SOC is depicted by a dashed line in Fig. 4; the triplet state with SOC account is shown by a dotted line. Actually, this state is almost a complete mixture of the $^3\Sigma_g^-$ and $^1\Sigma_g^+$ states.

The upper and lower singlet state surfaces studied by Balasubramanian [17] with the parallel mode of $Pt_2 + H_2$ collisions are presented in Fig. 4 by solid lines and their avoided crossing is shown schematically by dashed lines. The lower surface was found to be relatively flat for $4 \leq d \leq 8$ Å. Balasubramanian [17] calls it ''the small H–H distance surface'', since the optimized H–H bond lengths in the flat region of this surface were close to the equilibrium bond length of the H_2 molecule.

The upper singlet state curve starts from a long H–H distance limit; contrary to the lower curve, the optimized H–H bond length becomes shorter as d decreases from 6 Å, while in the lower curve, the H–H bond length increases as the molecules approach. The barrier for dissociation of the hydrogen molecule in the lower surface arises from the avoided crossing. Once the barrier is surmounted, a deep well comprising the *cis* geometry of the Pt_2H_2 product is formed [17]; this product relaxes to a more stable *trans*-adduct. Similar PES have been studied by Dai et al. [27] for hydrogen molecule activation by Pt_3 and Pd_3 clusters.

We have reproduced the PES of Ref. [17] with one principal disagreement: the upper PES does not correspond to the $Pt_2(^1\Sigma_g^+) + H + H$ state [17], but rather to a two-triplet particle $^1[Pt_2(^3\Sigma_g^-) + H_2(^3\Sigma_u^+)]$ limit. A combination of these two triplet states produces the singlet state under consideration as well as the triplet and quintet counterparts (not shown in Fig. 4). Balasubramanian [17] mentioned that at $d = 6$ Å, the separation between the lower and upper surfaces corresponds to the dissociation energy of the H_2 molecule. This was a simple consequence of the fact that the energy difference between the $^3\Sigma_g^-$ and $^1\Sigma_g^+$ states in the nonrelativistic calculation was negligible in comparison with the accuracy of the dissociation energy estimation.

The singlet and triplet $^1\Sigma_g^+$ and $^3\Sigma_u^+$ states of the hydrogen molecule H–H are degenerate at a large internuclear distance; the triplet state $^3\Sigma_g^-$ of Pt_2 is lower than the singlet $^1\Sigma_g^+$ state so our assignment is quite natural. The singlet state $Pt_2(^1\Sigma_g^+) + H + H$ assignment in Ref. [17] implies that the hydrogen radical pair is in the singlet $^1\Sigma_g^+$ state. This state leads to a fast recombination to the hydrogen molecule when the system is allowed to relax during the reaction path optimization. So it immediately converts into the lower potential energy singlet

surface when the H–H bond length was optimized during the reaction path search. Only the triplet state $^3\Sigma_u^+$ radical pair H + H is stable with respect to such geometry optimization at long intermolecular distances $d \simeq 6$–4 Å. In turn, only the triplet state ($^3\Sigma_g^-$) of platinum dimer can be combined with the hydrogen triplet in order to produce a singlet state which participates in the avoided crossing with the lower curve. Such type of spin uncoupling is a common feature of chemical bond activation by metal systems [30,35,37,38].

The same arguments are applied to hydrogen molecule activation by Pt_3 and Pd_3 clusters studied by Balasubramanian [17]. The ground state Pt_3 cluster is a triplet $^3A_1$ triangle of C_{2v} symmetry [39]. (Recent B3LYP calculations predict quasi-degenerate singlet and triplet states of similar geometries [22] for the Pt_3 cluster. The Palladium trimer has a triplet ground state with slightly higher S–T splitting [22].) The upper PES in Ref. [27] could again be attributed to the singlet state obtained by combination of the two triplet molecules. In fact, the energy differences between the upper and lower curves at the dissociation limit are not exactly equal to each other for the Pt_3H_2 and Pd_3H_2 systems. It means that the S–T energy gaps are not exactly the same for platinum and palladium trimers in the calculations of Dai et al. [27] (these values are not given in Ref. [27]). Though the full geometry optimization [21,22] leads to other reaction paths, the results of Balasubramanian [17] and Dai et al. [27] illustrate the importance of spin uncoupling induced by configuration interaction between the closed shell singlet state in the lower entrance channel and the double–triplet excited state Pt_n + H + H. This type of spin uncoupling could be present even in the full geometry optimization [21,22] though it is not seen in such an obvious manner like in the studies of Balasubramanian [17] and Dai et al. [27].

Many other TMs, their clusters and complexes, have a high-spin ground state; the excited low-spin states are often more reactive in catalytic processes. This can be easily understood as a result of a combination between having a high-spin state of a catalyst and the triplet excitation of an activated chemical bond (like the $^3\Sigma_u^+$ state of the H–H bond) in which the total spin of the catalytic system is lowered to the low-spin state. Such a combination is extremely reactive (as a diabatic state) and correlates always with the ground state of the insertion product on the correlation diagram for diabatic states [9,40]. The low-spin state reactivity is determined by an effective avoided crossing between the starting reactant term and this extremely reactive descending state. Finally, the high-spin–low-spin cross-coupling induced by SOC becomes the important driving force of catalytic activity. The simplest prototype of catalytic reactions, Pt + H_2, demonstrates all these features.

4. Conclusions

Recent calculations [2,5,8,24] show that the interaction between a TM atom at the right side of the periodic table and a diamagnetic closed shell molecule is reactive in the excited low-spin state and is nonreactive in the ground high-spin state. The same type of correlation diagram with the reactive low-spin state (singlet ^1S state in the case of the Pt atom) and nonreactive high-spin state (the Pt triplet ^3D state) can be easily obtained for other TMs with more than half occupied *d* shell and for their complexes. For example, the high-spin ground states of the Rh and Ru atoms (^4F and ^5F states, respectively) do not directly produce stable complexes with methane [5] and ethylene [41]. The complexes have the lower spin multiplicity, namely the doublet and triplet states for the complexes with Rh and Ru atoms, respectively [5,41]. For these atoms, an account of SOC becomes of crucial importance, since only SOC can govern their reactivity. The correlation diagram with involvement of the triplet excited methane and

ethylene can be easily reproduced by the CI method for these reactions.

The conclusions are not much changed going from the bare metal to metal clusters. Our results for the Pt_2 dimer interaction with methane indicate that SOC and the strong triplet–singlet repulsion are the main driving forces behind the C–H bond activation in this catalytic process.

The correlation diagram similar to the one shown in Fig. 4 could be applied for hydrocarbon interaction with Cu clusters and for the chemisorption models on Cu surfaces [38]. The high and low-spin states of the Cu clusters are very close in energy and they can be used instead of the triplet and singlet states of the Pt_2 dimer in Fig. 4. For example, our calculations illustrate a very strong interaction between the triplet excited ethylene and Cu_{14} cluster simulating the di–σ bridge model [38] of the chemisorption on the Cu(100) surface. The upper excited state behaviour clearly indicates the correlation diagram of the type shown in Fig. 4, though the ground state is a singlet closed shell system.

An important issue of the present work is connected with the qualitative understanding of the catalytic reactivity of the hydrogen molecule adsorbed on the surface. At the beginning of the interaction with the platinum surface, only one Pt atom is involved in the hydrogen activation. The spin uncoupling considered is relevant with inclusion of the triplet–singlet transition induced by SOC. The role of the catalyst is twofold: firstly, to incorporate a very strong SOC in the Pt atom in order to induce the triplet–singlet transition and, secondly, to involve the triplet excited H_2 molecule in the catalytic process.

References

[1] J. Chatt, L.A. Duncanson, J. Chem. Soc. (1953) 2939.
[2] J.J. Low, W.A. Goddard III, Organometallics 5 (1986) 609.
[3] P. Siegbahn, M.R.A. Blomberg, M. Svensson, J. Am. Chem. Soc. 115 (1993) 1952.
[4] M.R.A. Blomberg, P. Siegbahn, M. Svensson, J. Phys. Chem. 96 (1992) 5783.
[5] M.R.A. Blomberg, P. Siegbahn, M. Svensson, J. Am. Chem. Soc. 114 (1992) 6095.
[6] Z.M. Muldahmetov, B.F. Minaev, G.A. Ketsle, Optical and Magnetic Properties of the Triplet State, Nauka, Alma Ata, 1983, in Russian.
[7] H. Nakatsuji, Y. Matsuzaki, T. Yonesawa, J. Chem. Phys. 88 (1988) 5759.
[8] K. Balasubramanian, J. Chem. Phys. 87 (1987) 2800.
[9] B.F. Minaev, H. Ågren, Coll. Czechoslovak Chem. Commun. 60 (1995) 339.
[10] P.E.M. Siegbahn, J. Am. Chem. Soc. 118 (1996) 1487.
[11] A.M.C. Wittborn, M. Costas, M.R.A. Blomberg, P.E.M. Siegbahn, J. Chem. Phys. 107 (1997) 4318.
[12] A.E. Shilov, Activation of Saturated Hydrocarbons by Transition Metal Complexes, D. Riedel, Dordrecht, 1984.
[13] T. Fayet, A. Kaldor, D.M. Cox, J. Chem. Phys. 92 (1990) 254.
[14] D.J. Trevor, A. Kaldor, D.M. Cox, J. Am. Chem. Soc. 112 (1990) 3742.
[15] J.J. Low, W.A. Goddard III, J. Am. Chem. Soc. 108 (1986) 6115.
[16] K. Balasubramanian, P.Y. Feng, M.Z. Liao, J. Chem. Phys. 88 (1988) 6956.
[17] K. Balasubramanian, J. Phys. Chem. 94 (1991) 1253.
[18] K. Balasubramanian, J. Chem. Phys. 105 (1995) 7530.
[19] N. Koga, K. Morokuma, Chem. Rev. 91 (1991) 823.
[20] D.G. Musaev, K. Morokuma, J. Phys. Chem. 100 (1996) 11600.
[21] Q. Cui, D.G. Musaev, K. Morokuma, J. Chem. Phys. 108 (1998) 8414.
[22] Q. Cui, D.G. Musaev, K. Morokuma, J. Phys. Chem. 102A (1998) 6373.
[23] E. Poulain, J. Garcia-Prieto, M.E. Ruiz, O. Novaro, Int. J. Quantum Chem. 29 (1986) 1181.
[24] O. Swang, K. Faegri Jr., O. Gropen, J. Phys. Chem. 98 (1994) 3606.
[25] K. Balasubramanian, J. Phys. Chem. 93 (1989) 6585.
[26] C.E. Moore, Atomic Energy Levels, Vol. III, NBS, Washington, DC, 1958.
[27] D. Dai, D.W. Liao, K. Balasubramanian, J. Chem. Phys. 102 (1995) 7530.
[28] D. Dai, K. Balasubramanian, J. Chem. Phys. 103 (1995) 648.
[29] Z.M. Muldahmetov, B.F. Minaev, S.A. Beznosjuk, Electronic Structure of Molecules, New Aspects, Nauka, Alma Ata, 1988, in Russian.
[30] B.F. Minaev, H. Ågren, Int. J. Quantum Chem. 57 (1996) 510.
[31] W.J. Stevens, M. Krauss, H. Basch, P. Jasien, Can. J. Chem. 70 (1992) 612.
[32] S. Koseki, M.H. Schmidt, M.S. Gordon, J. Phys. Chem. 96 (1992) 10678.
[33] M.W. Schmidt, K.K. Baldridge, J.A. Boats, S.T. Elbert, M.S. Gordon, J.H. Jensen, S. Koseki, N. Matsunaga, K.A. Nguyen, S.J. Su, T.L. Windus, J. Comput. Chem. 14 (1993) 1347.
[34] W.J. Hehre, L. Radom, P. Schleyer, J.A. Pople, Ab Initio MO Theory, Wiley, New York, 1986.
[35] B.F. Minaev, H. Ågren, Int. J. Quantum Chem. (1999).

[36] K. Balasubramanian, J. Chem. Phys. 87 (1987) 6573.
[37] F. Mulder, G. van Dijk, C. Huiszoon, Mol. Phys. 38 (1973) 577.
[38] L. Triguero, L.G.M. Pettersson, B.F. Minaev, H. Ågren, J. Chem. Phys. 108 (1998) 1193.
[39] H. Wang, E.A. Carter, J. Phys. Chem. 96 (1992) 1197.
[40] B.F. Minaev, Khim. Fizika 3 (1984) 983.
[41] M.R.A. Blomberg, P. Siegbahn, M. Svensson, J. Phys. Chem. 96 (1992) 9794.